Int. J. Heat Mass Transfer. Vol. 27, No. 3, pp. 451–461, 1984
Printed in Great Britain

0017–9310/84 $3.00 + 0.00
Pergamon Press Ltd.

DROPLET FORMATION AND GROWTH IN CONDENSING BINARY VAPOURS

W. STUDZIŃSKI,† R. A. ZAHORANSKY, S. L. K. WITTIG and D. BARSCHDORFF‡
Lehrstuhl und Institut für Thermische Strömungsmaschinen,
Universität Karlsruhe, Kaiserstr. 12, 7500 Karlsruhe, Federal Republic of Germany

(*Received* 20 *December* 1982 *and in revised form* 30 *March* 1983)

Abstract—An earlier model of the droplet growth in unary condensation is extended for binary mixtures. The theoretical results are compared with measurements in the driver section of a shock tube using ethanol/water systems. Droplet radii and concentration are determined by means of the dispersion quotient technique. Particle size in the range of 0.1–1 μm and particle densities between 10^{11} and 10^{14} m^{-3} were determined. Theoretical and experimental results are in good agreement under the conditions chosen.

NOMENCLATURE

A	path length within test section of expansion tube
B_i	diffusion factor
c_i	mass fraction
c_{pi}	specific heat by constant pressure
C	frequency factor
D_{i0}	diffusion coefficient of vapour in inert gas
h	enthalpy of the gas mixture
H	total enthalpy of the gas mixture
I	light intensity of attenuated beam
j	diffusion flux
J	nucleation rate
k	Boltzmann's constant
K_i	molecule concentration
$\bar{l}$	mean free path
L_i	latent heat of pure component
m_i	mass of droplet component
$\dot{m}_i$	mass rate of condensing specie
M_i	molar mass
n_i	number of molecules in cluster
$\tilde{n}$	refractive index
N	particle concentration
p_i	partial pressure
p_{si}	equilibrium vapour pressure over solution
p_{si}°	equilibrium vapour pressure over pure liquid component
Q_{ext}	extinction cross section
r	droplet radius
R	universal gas constant
R_i	individual gas constant
S_i	supersaturation of component
t	time
T	temperature
$\mathbf{U}$	gas velocity connected with condensation
v	partial molar volume
w	molecule mass
x	coordinate along shock tube
X	mole fraction of component
Z	Zeldovich factor.

Greek symbols

α	heat conductivity number for sphere
β_i	impingement rate
γ_i	activity coefficient
δ_i	coefficient, equation (51)
η	radial coordinate
$\bar{\kappa}$	isentropic exponent for the gas mixture
λ_i	thermal conductivity of gaseous component
$\lambda_{I,II}$	light wavelength
μ_i	partial chemical potential per molecule
$\bar{\mu}$	dynamic viscosity of the gas mixture
ρ_i	density
σ	bulk surface tension of solution
ω	coefficient, equation (64).

Subscripts

i	component 1 or 2
j	droplet class
0	carrier gas
1	water
2	ethanol
r	droplet surface
∞	ambient vapour parameter
*	metastable equilibrium
obs	observation station.

Superscripts

$''$	gas phase
$'$	liquid phase
+	at boundary of Knudsen layer
$\circ$	pure component
$\bar{}$	average value.

1. INTRODUCTION

DUE TO its growing importance in various application such as energy conversion and in the analysis c meteorological processes, binary nucleation an condensation has been met with growing interest. Fo

† Instytut Maszyn Przepływowych PAN, ul. Fiszera 14, 80-952 Gdańsk, Poland, research fellow of the Alexander von Humboldt Foundation.

‡ Fachgebiet Elektrische Meßtechnik, Universität -GH Paderborn, Pohlweg 47-49, 4790 Paderborn, Federal Republic of Germany.

example, Bodmer [1] and Bohnsack [2] directed their attention to the influence of trace elements in the feed water of power plants with primary emphasis on the condensation phenomena and subsequent erosion and corrosion in steam turbines. An attempt was made to explain qualitatively some of the observed damages by an enrichment of the condensed water droplets with other components such as acetic acid and silicic acid. On the other hand, the enrichment of raindrops by atmospheric impurities, e.g. sulphuric acid, have become of public concern. Up to now only the nucleation processes as a first step in homogeneous binary condensation have been studied. Doyle [3] and Mirabel and Katz [4] used the original assumptions by Flood [5] and Reiss [6], who considered steady-state nucleation. Stauffer [7] studied the influence of polluting reactants in water condensation. High nucleation rates were predicted theoretically even for water activities below one. As mixtures with components such as sulphuric acid in water lead to extremely small partial pressures, ethanol/water [8] or n-propanol/water [9] were used for comparison with theory. Observed discrepancies between theory and experiment with water rich mixtures were explained by surface enrichment effects by alcohol molecules as the surface tension of pure water is altered drastically by small amounts of alcohol.

Only limited information is available on droplet growth in binary vapours. First models were proposed by Kaser [10], Fukuta and Walter [11], Dingle [12] and Meyer [13], however, no experimental verification was obtained. This paper, therefore, is directed towards the theoretical analysis of this process and its experimental proof. Using the conservation equations for single binary drops in a surrounding gas, it is shown that the droplet temperature can be eliminated. The diffusion of vapours through an inert carrier gas is taken into account—as required for an extended Maxwell–Mason type model.

The theoretical results are compared with measurements of water/ethanol mixtures in the rarefaction wave of a shock tube. Opto-electronic diagnostics—i.e. dispersion quotient technique—is applied in determining the particle size and concentration as a function of time.

2. NUCLEATION

The computation of a flow with condensation contains three main elements:

(1) the nucleation rate equation for newly formed nuclei;

(2) the equations for droplet growth, change of composition and temperature;

(3) the gas dynamic equations for the surrounding vapour phase of the droplet.

The initial conditions for the computation of droplet growth are predicted from nucleation theory. For binary condensation, the knowledge of the initial number of nuclei, their size and composition is required. Embryo size and composition are derived from the conditions of the thermodynamic metastable equilibrium. The free energy necessary to form a nucleus of arbitrary size and composition is given by [14]

$$\Delta G = n_1\Delta\mu_1 + n_2\Delta\mu_2 + 4\pi r^2\sigma(X_2', T) + (n_1+n_2)(p-p_s)v, \quad (1)$$

where

$$v = X_1'v_1 + X_2'v_2,$$

$$X_1' = n_i/(n_1+n_2),$$

$$\Delta\mu_i = \mu_i' - \mu_i'' = -kT\ln\frac{p_i}{p_{si}},$$

$$p_{si} = p_{si}^{\circ}X_i'\gamma_i(X_i', T).$$

The last term in equation (1) can be neglected as it is very small compared to the other terms for moderate supersaturations of interest here. The necessary conditions of metastable equilibrium are [15]

$$\left(\frac{\partial\Delta G}{\partial n_1}\right)_{n_2} = 0, \qquad \left(\frac{\partial\Delta G}{\partial n_2}\right)_{n_1} = 0 \quad (2)$$

and

$$\frac{\partial^2\Delta G}{\partial n_1\,\partial n_2} - \frac{\partial^2\Delta G}{\partial n_1^2}\frac{\partial^2\Delta G}{\partial n_2^2} > 0.$$

This set of equations characterizes the saddle point condition of the energy surface $\Delta G(n_1, n_2)$ and leads to nonlinear algebraic equations for droplet radius and composition

$$\Delta\mu_1 + \frac{2\sigma v_1}{r} - \frac{3X_2'v}{r}\frac{\partial\sigma}{\partial X_2'} = 0, \quad (3)$$

$$\Delta\mu_2 + \frac{2\sigma v_2}{r} + \frac{3(1-X_2')v}{r}\frac{\partial\sigma}{\partial X_2'} = 0, \quad (4)$$

these equations together with the relation for the radius

$$\tfrac{4}{3}\pi r^3 = (n_1+n_2)v, \quad (5)$$

defines the droplet size and composition in the saddle point. This pass is the energy barrier the clusters have to overcome in order to become stable.

The rate of homogeneous nucleation in a binary mixture is predicted by [3]

$$J = C\exp\left(-\frac{\Delta G_*}{kT}\right). \quad (6)$$

The frequency factor C was derived by Reiss [6] from reaction kinetics

$$C = \frac{\beta_1\beta_2}{\beta_1\sin^2\phi + \beta_2\cos^2\phi}(K_1+K_2)4\pi r^2 Z, \quad (7)$$

where

$$\beta_i = \frac{p_i}{\sqrt{(2\pi w_i kT)}},$$

$$K_i = p_i/kT,$$

$$Z = \sqrt{(-P/Q)}.$$

Here ϕ is the angle between the projected nucleation path direction in the n_1, n_2 plane to the n_1-axis, P and Q the second derivatives of ΔG with respect to the new rotated axis in the direction of the main nucleation path and perpendicular to that one

$$P = \left(\frac{\partial^2 \Delta G}{\partial n_1^2}\right)\cos^2\phi + 2\left(\frac{\partial^2 \Delta G}{\partial n_1\,\partial n_2}\right) \times \cos\phi\,\sin\phi + \left(\frac{\partial^2 \Delta G}{\partial n_2^2}\right)\sin^2\phi, \quad (8)$$

$$Q = \left(\frac{\partial^2 \Delta G}{\partial n_1^2}\right)\sin^2\phi - 2\left(\frac{\partial^2 \Delta G}{\partial n_1\,\partial n_2}\right) \times \sin\phi\,\cos\phi + \left(\frac{\partial^2 \Delta G}{\partial n_2^2}\right)\cos^2\phi. \quad (9)$$

The second derivatives of ΔG with respect to n_1 and n_2 are obtained following Mirabel and Katz [4], for example. In considering the differential arrival rates of the condensing species at the embryo surface, the nucleation path deviates from the direction of steepest descent on the energy surface and the angle of rotation is given by Stauffer [7]:

$$\tan^2\phi + (f d_B - d_A)\cdot\tan\phi - f = 0, \quad (10)$$

where $f = \beta_2/\beta_1$ is the correction factor

$$d_A = -\frac{\partial^2 \Delta G}{\partial n_1^2}\Big/\frac{\partial^2 \Delta G}{\partial n_1\,\partial n_2}, \quad (11)$$

$$d_B = -\frac{\partial^2 \Delta G}{\partial n_2^2}\Big/\frac{\partial^2 \Delta G}{\partial n_1\,\partial n_2}. \quad (12)$$

3. MODEL OF DROPLET GROWTH

The growth of binary drops was theoretically investigated by Fukuta and Walter [11], Kaser [10], Mirabel and Katz [4], Dingle [12], and Meyer [13]. Dingle's model is based on a modified Maxwell diffusion equation for two components coupled with the energy balance of the droplet. This system is referred to as the explicit model as the droplet temperature equation is explicitly required to solve the diffusion equation.

Kaser's explicit equations of the droplet growth are derived from the mass and energy balance in the Knudsen layer around the droplet surface and from diffusion and energy equations in the surrounding vapour sphere.

No information on the droplet composition is obtained using Fukuta and Walter's implicit droplet growth model. Improvements proposed by Meyer allow the computation of droplet composition. The algebraic equation for its temperature, however, is used in explicit form. Mirabel and Katz's model is limited to the case, where one component is highly diluted.

One of the purposes of this paper is to develop an advanced implicit model whereby the growth, composition and droplet temperature equations are combined into a growth and composition equation that depends only upon the supersaturation ratios. The influence of droplet temperature on condensation is taken implicitly into consideration.

The droplet with radius r and composition X_1' is considered in a surrounding vapour sphere. The influence of adjacent drops and droplet slip is neglected. The gas phase consists of two condensing gases with partial pressures $p_{12} = p_1 + p_2$ and of a non-condensable inert gas with partial pressure p_0.

The condensing components form a real solution and are diluted with the inert gas

$$p_0 \gg p_1 + p_2. \quad (13)$$

In a good approximation, the pressure around the drop is constant and equal to the pressure at infinity ($\eta \to \infty$)

$$p(\eta) = p_\infty = \text{const.}, \quad (14)$$

where η is the radial coordinate.

By assuming an independent diffusion, the change of mass $m = m_1 + m_2$ of a binary droplet may be expressed as

$$\frac{dm}{dt} = \frac{dm_1}{dt} + \frac{dm_2}{dt} = \dot{m}_1 + \dot{m}_2. \quad (15)$$

For moderate pressure levels of interest the behaviour of the vapours and the carrier gas is assumed to be perfect

$$p_i = \rho_i'' R/M_i T. \quad (16)$$

If the change of external flow parameters is not too fast, the transport phenomena in the gas sphere surrounding the drop can be treated as stationary and the conservation equations yield

$$\operatorname{div}(\rho''\mathbf{U}) = 0, \quad (17)$$

$$\operatorname{div}(\rho_1''\mathbf{U}) = -\operatorname{div}\mathbf{j}_1, \quad (18)$$

$$\operatorname{div}(\rho_2''\mathbf{U}) = -\operatorname{div}\mathbf{j}_2, \quad (19)$$

$$\rho''\frac{dH}{dt} = \operatorname{div}(\bar{\lambda}\ \operatorname{grad}\ T), \quad (20)$$

where

$$\bar{\lambda} = c_0''\lambda_0 + c_1''\lambda_1 + c_2''\lambda_2,$$

$$c_i'' = \frac{\rho_i''}{\rho_0'' + \rho_1'' + \rho_2''}. \quad (21)$$

The influence of diffusion on energy transport is insignificant. Due to smooth gradients of pressure and temperature, the pressure-diffusion and thermo-diffusion effects can be neglected in the relation for mass fluxes $\mathbf{j}_1$ and $\mathbf{j}_2$

$$\mathbf{j}_1 = \rho'' D_{10}\ \operatorname{grad}\ c_1'', \quad (22)$$

$$\mathbf{j}_2 = \rho'' D_{20}\ \operatorname{grad}\ c_2''. \quad (23)$$

In radial coordinates the set of equations (17)–(20) will be more convenient for integration. Taking into account boundary conditions for $\eta = r$ one obtains

$$4\pi r^2(\rho_1'' U + j_1) = -\dot{m}_1, \quad (24)$$

$$4\pi r^2(\rho_2'' U + j_2) = -\dot{m}_2, \tag{25}$$

$$4\pi r^2 \rho'' U = -(\dot{m}_1 + \dot{m}_2), \tag{26}$$

$$\bar{\lambda}\left(\frac{dT}{d\eta}\right)_r = -\frac{\dot{m}_1 L_1 + \dot{m}_2 L_2}{4\pi r^2}. \tag{27}$$

The droplet temperature T_r is approximated by a time-dependent step function ($dT_r/dt = 0$, $T_r(t) \neq$ const.) because the change of the internal droplet energy is significant only during extremely fast expansions [16]. An additional phenomenon of minor influence is radiative transfer from the drop, surface increase energy and heat of dilution will be omitted in this model [equation (27)].

Single integration of conservation equations (17)–(20) leads to

$$\eta^2 \rho'' U = a_{12}, \tag{28}$$

$$\eta^2 \rho_1'' U = -\eta^2 j_1 + a_1, \tag{29}$$

$$\eta^2 \rho_2'' U = -\eta^2 j_2 + a_2, \tag{30}$$

$$a_{12} h = \eta^2 \bar{\lambda} \frac{dT}{d\eta} + b_{12}, \tag{31}$$

where

$$h = h_0 + \bar{c}_p T,$$

$$\bar{c}_p = c_0'' c_{p0} + c_1'' c_{p1} + c_2'' c_{p2}.$$

The integration constants are defined as

$$\begin{aligned} a_1 &= -\dot{m}_1/4\pi, \qquad a_2 = -\dot{m}_2/4\pi, \\ a_{12} &= a_1 + a_2, \qquad b_{12} = -(\dot{m}_1 L_1 + \dot{m}_2 L_2)/4\pi. \end{aligned} \tag{32}$$

The latent heat release and conductive heat transfer from the drop are dominant terms and exceed others by orders of magnitude. This fact allows the elimination of the droplet temperature equation in the implicit model of growth. It should be emphasized that the solution of the energy equation (31) predicts the drop temperature T_r with good accuracy as a step function.

In combining equations (28)–(30) the following relations between condensation rates $\dot{m}_i$ and diffusion fluxes j_i are obtained

$$\frac{\dot{m}_1}{4\pi\eta^2} = -\frac{(1-c_2'')j_1 + c_1'' j_2}{(1-c_2'')(1-c_1'') - c_1'' c_2''}, \tag{33}$$

$$\frac{\dot{m}_2}{4\pi\eta^2} = -\frac{(1-c_1'')j_1 + c_2'' j_2}{(1-c_1'')(1-c_2'') - c_1'' c_2''}. \tag{34}$$

In addition for fluid dynamic applications it is desirable to derive analytical solutions. With the assumption of equation (13) and relations (22) and (23), equations (33) and (34) lead to

$$\frac{\dot{m}_1}{4\pi\eta^2} = D_{10}\rho'' \frac{dc_1''}{d\eta}\Big/(1-c_1''), \tag{35}$$

$$\frac{\dot{m}_2}{4\pi\eta^2} = D_{20}\rho'' \frac{dc_2''}{d\eta}\Big/(1-c_2''), \tag{36}$$

where

$$\bar{R} = \sum_{i=0}^{2} c_i'' R_i.$$

For $\rho'' = \rho_\infty''$ and with the Taylor expansion of the exponential term

$$\exp\left(\frac{\dot{m}_i}{4\pi\eta}\frac{\bar{R}T_\infty}{p_\infty D_{i0}}\right) \simeq 1 + \frac{\dot{m}}{4\pi\eta}\frac{\bar{R}T_\infty}{p_\infty D_{i0}},$$

the integrals of equations (35) and (36) simplify for $\eta = r$ to

$$\frac{\dot{m}_i}{4\pi r^2} = B_i^+(p_{i\infty} - p_{ir}), \tag{37}$$

where

$$B_i^+ = \frac{D_{i0}/(1-c_{i\infty}'')}{rR_iT_\infty}. \tag{38}$$

Similarly, the solution of the linear energy equation (31) is obtained neglecting second-order terms.

For $\eta = r$:

$$T_r - T_\infty = \frac{\dot{m}_1 L_1 + \dot{m}_2 L_2}{4\pi r\bar{\lambda}} = \frac{\dot{m}_1 L_1 + \dot{m}_2 L_2}{\alpha_\kappa 4\pi r^2}, \tag{39}$$

where

$$\alpha_\kappa = \frac{\bar{\lambda}}{r}, \tag{40}$$

is the heat conductivity number for a sphere. This number refers to the conductivity in a continuum. For droplets smaller than the mean free path $\bar{l}$, Gyarmathy [17] proposed a correction factor for α_κ

$$\alpha = \alpha_\kappa \cdot f\left(\frac{\bar{l}}{2r}\right) = \frac{\alpha_\kappa}{1 + 3.18\bar{l}/2r} = \frac{\bar{\lambda}}{r + 1.59\bar{l}}. \tag{41}$$

In analogy for the diffusion factor B_i^+

$$B_i = B_i^+ \cdot f\left(\frac{\bar{l}}{2r}\right) = \frac{D_{i0}/(1-c_{i\infty}'')}{(r+1.59\bar{l})R_iT_\infty}. \tag{42}$$

The mean free path can be estimated as

$$\bar{l} = 1.5\bar{\mu}\sqrt{(\bar{R}T_\infty)}/p_\infty, \tag{43}$$

where $\bar{\mu}$ is the mean dynamic viscosity of the gas mixture.

The partial pressure of the components in the drop can be calculated starting from Laplace's equation in differential form

$$dp_r - dp = d\left(\frac{2\sigma}{r} + \frac{\partial\sigma}{\partial r}\right). \tag{44}$$

Using the thermodynamic derivatives of chemical potential

$$\left(\frac{\partial\mu_i'}{\partial p}\right)_T = v_i, \tag{45}$$

with equilibrium conditions $d\mu_i' = d\mu_i''$ one obtains

$$kT \ln\frac{p_{ir}}{p_{si}} = v_i\left(\frac{2\sigma}{r} + \frac{\partial\sigma}{\partial r}\right). \tag{46}$$

The integration of equation (44) was carried out for ideal gases and by neglecting the liquid's compressibility.

The derivatives of σ with respect to X_i' can be obtained from equation (5)

$$\left(\frac{\partial r}{\partial X_i'}\right)_{n_i} = -\frac{r v_i}{3 v X_i'} \tag{47}$$

$$\left(\frac{\partial \sigma}{\partial r}\right)_{T,X_i'} = \left(\frac{\partial \sigma}{\partial X_i'}\right)_T \left(\frac{\partial X_i'}{\partial r}\right)_{n_i}. \tag{48}$$

For binary mixtures $\partial/\partial X_2' = -\partial/\partial X_1'$.

The equilibrium over the curved surface p_{ir} is equal to

$$\frac{p_{ir}}{p_{si}} = \exp\left[\left(\frac{2\sigma v_i}{r} + \frac{3(1-X_i')v}{r}\frac{\partial \sigma}{\partial X_i'}\right)\Big/(kT)\right]. \tag{49}$$

These equations are identical with the saddle point conditions, equations (3) and (4), for metastable equilibrium. Assuming that relation (49) is approximately valid also for nonequilibrium growth of droplets, the pressure p_{ir} can be expressed in terms of the radius and composition of critical droplets:

$$\ln\frac{p_{ir}}{p_{si}^\circ(T_r)\gamma_{ir}X_{ir}'} = \frac{r_*}{r}\frac{T}{T_r}\delta_i \ln\frac{p_{i\infty}}{p_{si}^\circ(T)\gamma_{i*}X_{i*}'}, \tag{50}$$

$$\delta_i = \frac{v_{ir} + 1.5(1-X_{ir}')v_r(\partial \ln \sigma/\partial X_i')_r}{v_{i*} + 1.5(1-X_{i*}')v_*(\partial \ln \sigma/\partial X_i')_*}. \tag{51}$$

The temperature ratio T/T_r is close to unity. To obtain the droplet growth equations in a convenient form, the solutions of the diffusion equation (37) and the energy equation (39) should be connected and expressed as functions of component activities in the gas phase or component supersaturations. The activities, therefore, must be transformed

$$\ln\frac{p_{i\infty}}{p_{si}^\circ(T_\infty)} = \ln\frac{p_{i\infty}}{p_{ir}} + \ln\frac{p_{ir}}{p_{si}^\circ(T_r)} + \ln\frac{p_{si}^\circ(T_r)}{p_{si}^\circ(T_\infty)}. \tag{52}$$

Here the term $p_{i\infty}/p_{ir}$ is approximately unity. Linearization and combination with equation (37) yields

$$\ln\frac{p_{i\infty}}{p_{ir}} \simeq 1 - \frac{1}{p_{i\infty}/p_{ir}} = \frac{\dot{m}_i}{B_i 4\pi r^2}\frac{1}{p_{i\infty}}. \tag{53}$$

The second term of equation (52) is defined by equation (50) and the last one is estimated by the linear term of a Taylor series expansion

$$\ln\frac{p_{si}^\circ(T_r)}{p_{si}^\circ(T_\infty)} = \left.\frac{\mathrm{d}\ln p_{si}^\circ(T)}{\mathrm{d}T}\right|_\infty (T_r - T_\infty). \tag{54}$$

With the ideal gas assumption, the derivative of $\ln p_{si}^\circ$ vs temperature is given by the Clausius–Clapeyron equation

$$\left.\frac{\mathrm{d}\ln p_{si}^\circ}{\mathrm{d}T}\right|_\infty = \frac{L_i}{R_i T_\infty^2}. \tag{55}$$

Equation (54) with energy equation (39) gives

$$\ln\frac{p_{si}^\circ(T_r)}{p_{si}^\circ(T_\infty)} = E_i(\dot{m}_1 L_1 + \dot{m}_2 L_2), \tag{56}$$

where

$$E_i = \frac{L_i}{R_i T_\infty^2 \alpha}. \tag{57}$$

Finally, from equation (52) with equations (50), (53), and (56) a system of two linear algebraic equations for the mass rates $\dot{m}_1$ and $\dot{m}_2$ is obtained, leading to the differential equations for the growth and the change of binary droplet composition

$$\frac{\dot{m}_1}{4\pi r^2} = F_1\left[\ln(S_1/S_2^\omega) - \frac{r_*}{r}(\delta_1 \ln S_{1*} - \delta_2 \ln S_{2*}^\omega)\right], \tag{58}$$

$$\frac{\dot{m}_2}{4\pi r^2} = F_2\left[\ln S_2 - \frac{r_*}{r}\delta_2 \ln S_{2*} - \frac{\dot{m}_1}{4\pi r^2} L_1 E_2\right], \tag{59}$$

where

$$S_i = \frac{p_{i\infty}}{p_{si}^\circ \gamma_i X_i'}, \tag{60}$$

$$S_{i*} = \frac{p_{i\infty}}{p_{si}^\circ \gamma_{i*} X_{i*}'}, \tag{61}$$

$$F_1 = \left[\frac{1}{p_1 B_1} + L_1 E_1 (1 - L_2 E_2 F_2)\right]^{-1}, \tag{62}$$

$$F_2 = \left(\frac{1}{p_2 B_2} + L_2 E_2\right)^{-1}, \tag{63}$$

$$\omega = L_2 E_1 F_2. \tag{64}$$

The masses of components in the drop m_1, m_2 are related to drop radius and composition as

$$r = \left[\left(\frac{m_1}{w_1} + \frac{m_2}{w_2}\right)v\right]^{1/3}, \tag{65}$$

$$X_2' = \frac{m_2/w_2}{m_1/w_1 + m_2/w_2}. \tag{66}$$

The implicit model developed may be applied to real as well as ideal mixtures in the liquid phase. The mass rates are dominantly dependent on the species supersaturations S_i.

4. EXPERIMENTAL TECHNIQUES

The study of binary condensation demands an extremely accurate preparation of the composition of the vapour mixtures. Only small amounts of condensing materials are required in the shock tube and arbitrary solutions can be supplied without problems.

Prior to an experiment, the heated shock tube (Fig. 1) is evacuated. The liquid test mixture is injected, vaporized and superheated within the driver section. Carrier gas is filled and mixed with the test fluid by means of a thin perforated tube mounted within this section. The state along the tube before firing is determined by means of six thermocouples and a static pressure transducer.

The static pressure during the unsteady expansion is

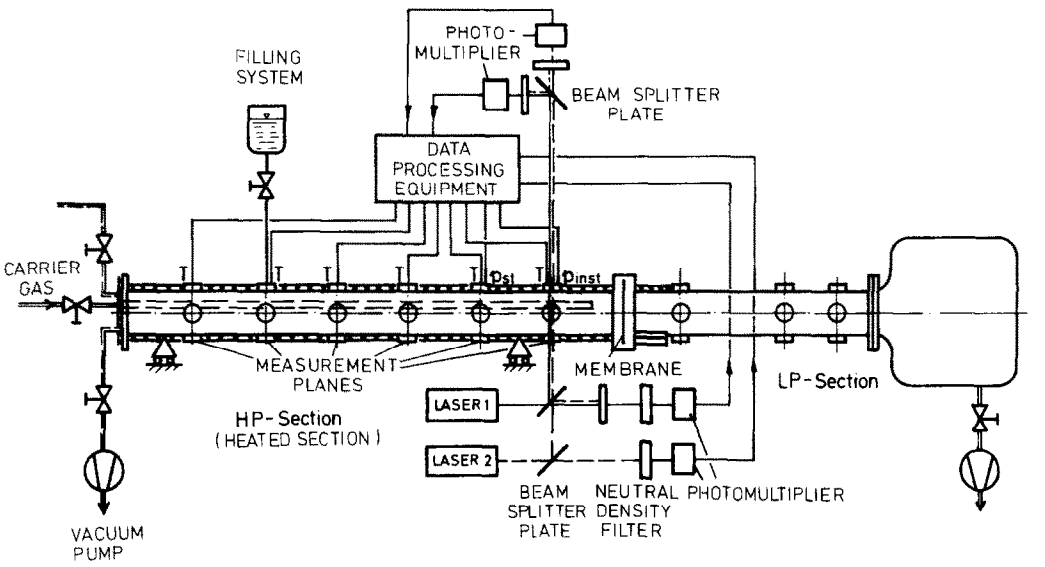

FIG. 1. Schematic of shock tube with measurement arrangement.

recorded by a Kistler quartz transducer, and the onset of homogeneous condensation is notified by measurements of light extinction.

Only an integrating optical method is applicable due to the short measurement time and high droplet concentration. For sufficiently diluted particle systems, multiple scattering can be neglected [18]. The chosen dispersion quotient technique was originally proposed by Teorell [19], and its application has been recently described in detail by Lester and Wittig [20], and Barschdorff *et al.* [21].

A monochromatic beam with intensity I_0 passing through an array of spheric particles is attenuated to

$$I = I_0 \exp[-N\pi r^2 Q_{ext}(r, \lambda, \tilde{n})A]. \qquad (67)$$

The droplet concentration N and the radius r are unknown. The radius r is obtained from the intensity ratios at two different wavelengths λ_I, λ_{II}

$$DQ = \frac{\ln(I/I_0)_I}{\ln(I/I_0)_{II}} = \frac{Q_{ext}(r, \lambda_I, \tilde{n}_I)}{Q_{ext}(r, \lambda_{II}, \tilde{n}_{II})}. \qquad (68)$$

For particles in the Mie range the dispersion quotient DQ decreases with size until the oscillatory scattering efficiency is reached (Fig. 2), and the particle size can easily be determined by equation (68). The computation of the extinction cross section is provided by the Mie theory. For polydisperse particles, the volume averaged radius will be approximately determined in the Mie range under consideration.

The procedure has been tested using monodisperse latex particles suspended in water [22]. The latex particle diameters were less than 1 μm and the concentration was varied between 10^{13} and 10^{18} particles m^{-3}. The excellent agreement between the predictions and measurements is demonstrated in Fig. 3.

Argon and helium–neon lasers were used as light sources. The refractive index is a function of wavelength and mixture composition. The attenuated light intensity was measured by two photomultipliers with impedance followers and monitored by a transient-recorder. Pressure and light intensity distributions

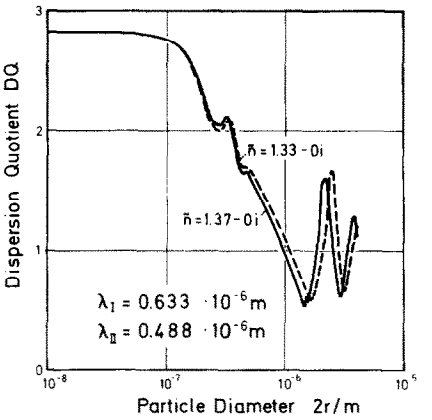

FIG. 2. Dispersion quotient DQ plotted vs droplet diameter for water $\tilde{n} = 1.33$ and water–ethanol mixture ($X'_2 = 0.8$) with maximum value $\tilde{n} = 1.37$.

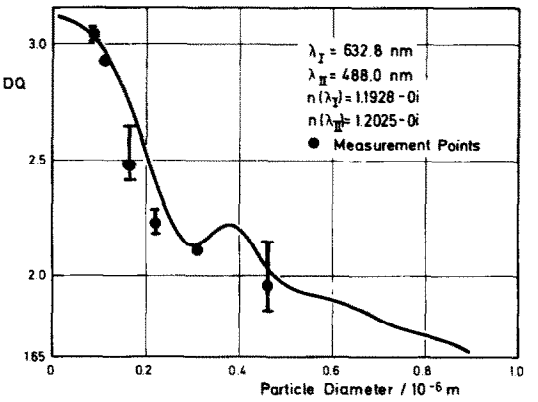

FIG. 3. Dispersion quotient for monodispersed latex particles in water suspension. Theory and experiment [22].

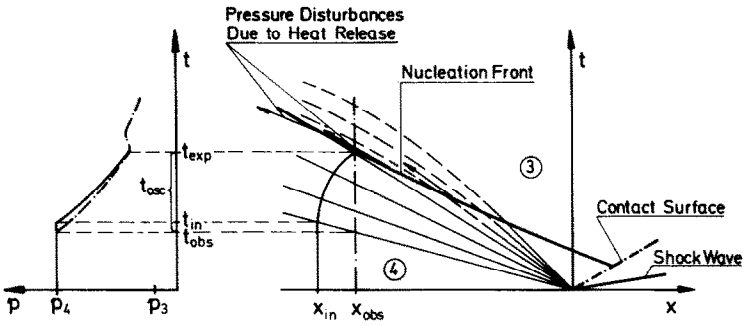

FIG. 4. Flow in unsteady rarefaction wave with condensation (schematic).

were also displayed on an oscilloscope triggered by a quartz pressure transducer.

5. FLOW IN UNSTEADY RAREFACTION WAVE

To show the validity of the model, measurements of droplet growth and concentration are performed in the driver section of a shock tube. In the case of an expansion without phase transition, the flow field in the unsteady rarefaction wave is well known from basic gasdynamics. The flow with binary nucleation and condensation requires the solution of a system of partial differential equations for the expansion wave simultaneously with the equations for nucleation and droplet growth similar to unary condensation [23]. This procedure is time consuming especially for binary drops, and the theoretical results are not satisfactory [24].

The simpler method, therefore, proposed by Barschdorff [25] will be used. The gasdynamic parameters necessary for nucleation, equation (6), and mass rates, equations (58) and (59), are computed by means of the method of characteristics for an unsteady expansion wave in a perfect gas. The method is applicable only if the influence of the latent heat on the flow is negligible, i.e. for mass fraction of the liquid phase

$$c_1' + c_2' \leqslant 10^{-3}. \tag{69}$$

The binary mixture of condensing media is diluted in an inert gas and is expanded adiabatically below the saturation state until the homogeneous condensation occurs and the supersaturation collapses.

The pressure history of the gas vapour mixture in the expansion wave can be expressed as a function of the characteristic slope x/t

$$\frac{p(t)}{p_4} = \left[1 + \frac{\bar{\kappa}_4 - 1}{\bar{\kappa}_4 + 1}\left(\frac{x/t}{\sqrt{(\bar{\kappa}_4 \bar{R} T_4)}} - 1\right)\right]^{2\bar{\kappa}_4/(\bar{\kappa}_4 - 1)} = \left(\frac{2}{\bar{\kappa}_4 + 1} + \frac{\bar{\kappa}_4 - 1}{\bar{\kappa}_4 + 1}\frac{t_{obs}}{t + t_{obs}}\right)^{2\bar{\kappa}_4/(\bar{\kappa}_4 - 1)}, \tag{70}$$

where $\bar{\kappa}_4$ is the isentrop exponent for the gas mixture; subscript 4 indicates initial conditions in the driver section before tube firing.

The pressure measurements are performed at a fixed test station.

The computation of condensation is carried out along the particle path which is obtained by integrating the local fluid velocity

$$x(t) = -t\frac{\sqrt{(\bar{\kappa}_4 \bar{R} T_4)}}{\bar{\kappa}_4 - 1}\left[2 - (\bar{\kappa}_4 + 1)\left(\frac{t_{in}}{t}\right)^{(\bar{\kappa}_4 - 1)/(\bar{\kappa}_4 + 1)}\right]. \tag{71}$$

The appropriate times t_{in} and t are obtained from the recorded pressure trace shown in Fig. 4.

It should be noted that in our experiments a virtual displacement of the origin of the characteristics is caused by a Laval nozzle installed at the entrance to the driven section. The nozzle dampens the disturbances due to heat release by impeding the propagation of the disturbances into the expansion fan from the low pressure section and around the diaphragm. The pressure increase under identical initial conditions using the nozzle generally occurs without a preceding shock wave [Fig. 5(a)] in contrast to the flow of the straight, circular shock tube [Fig. 5(b)].

The pressure increase and the light extinction in general are time-consistent.

6. EXPERIMENTAL RESULTS AND CRITICAL COMPARISON WITH THEORY

As mentioned earlier water/ethanol mixtures diluted with nitrogen were studied for comparison with the theoretical model. In general, initial conditions for the total pressure and temperature were held at approximately 2 bar and 313 K, respectively.

A typical record of the light extinction at the two wavelengths of 633 and 488 nm and the pressure trace is shown in Fig. 6. Corrections for the characteristic diagram (t_{obs}, x_{obs}) are taken into account in evaluating the proper conditions prior to the collapse of the supersaturated state.

The activities for onset of nucleation conditions are in excellent agreement with our previous results, Fig. 7 [8]. The observed droplet growth and change of concentration are shown in Figs. 8 and 9 for different initial concentrations within the vapour mixture. It can be seen that the computed pressure history agrees well with the experimental data whereas the calculated droplet growth is only satisfactory for a high initial ethanol concentration ($X_2'' > 0.5$).

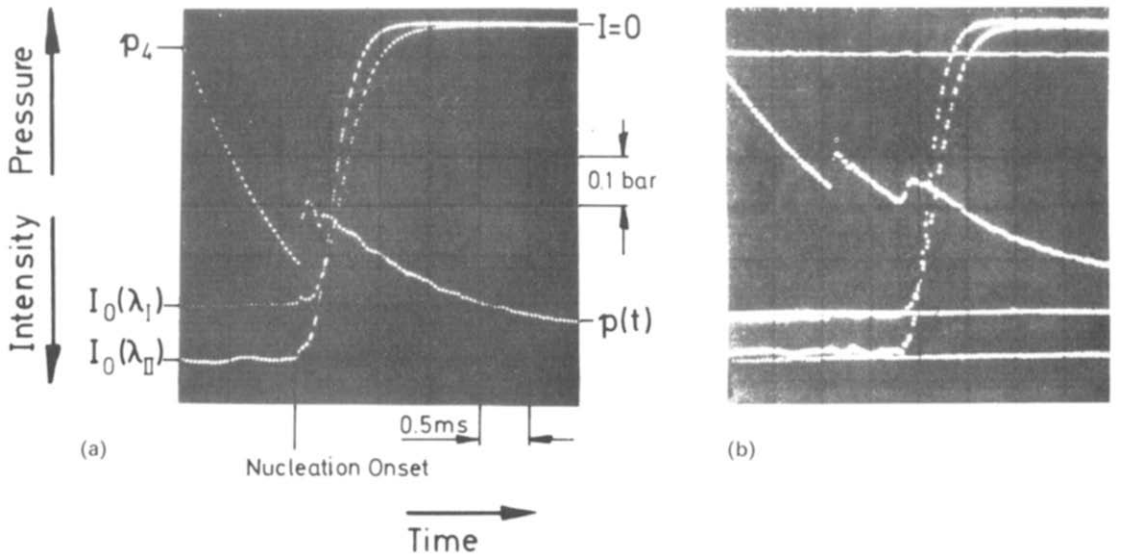

FIG. 5. Pressure and light extinction oscillograms for water–ethanol condensation in shock tube with (a) rectangular set and (b) without it.

At low alcohol concentrations (see Fig. 9) discrepancies between the model and the experimental results are observed as expected. For example the calculated onset of condensation and droplet growth is considerably earlier than that experimentally observed. The difficulty in utilizing the nucleation theory for mixtures with a drastically changing surface tension as a function of composition has been discussed by Mirabel and Katz [26] and could be responsible for the observed behaviour. Furthermore, the carrier gas effects on nucleation [25] are still under discussion.

It should be noted that the integration of the droplet growth equations [equations (58) and (59)] along the particle path is started by a sufficiently large nucleation rate J.

To speed up the integration, slightly higher than the critical values are chosen for the initial droplet size. Furthermore, it is assumed for the jth class of drops that the initial conditions are:

$$\begin{aligned} &\text{for } \phi_j < \frac{\pi}{4}, && n_{1j} = n^*_{1j} + 1, \\ &&& n_{2j} = n^*_{2j} + \cot\,\phi_j; \\ &\text{for } \phi_j > \frac{\pi}{4}, && n_{1j} = n^*_{1j} + \cot\,\phi_j, \\ &&& n_{2j} = n^*_{2j} + 1. \end{aligned} \tag{72}$$

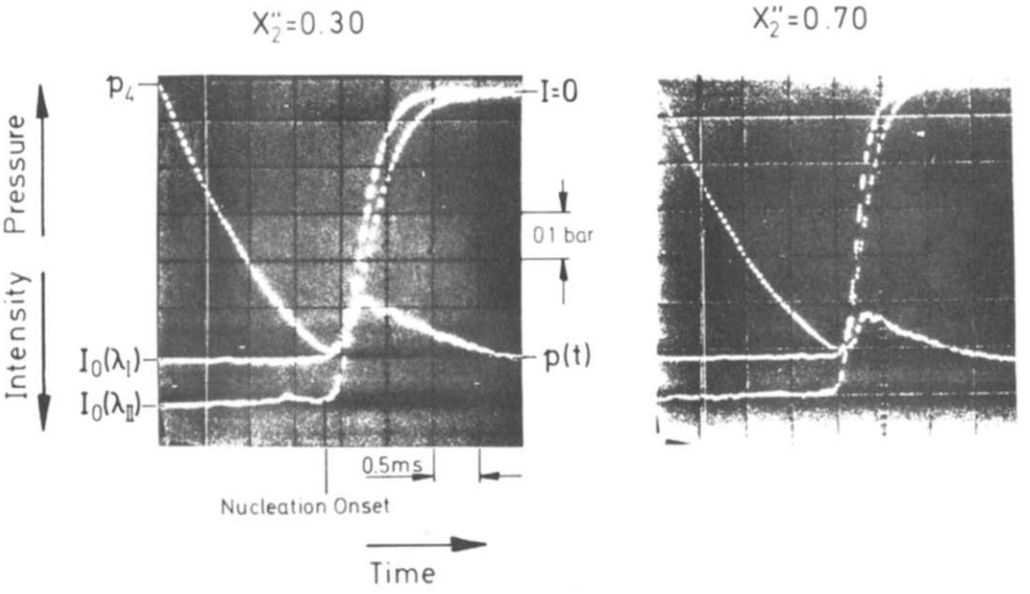

FIG. 6. Pressure and extinction signal traces for condensation of water–ethanol mixtures (see detailed analysis in Figs. 8 and 9).

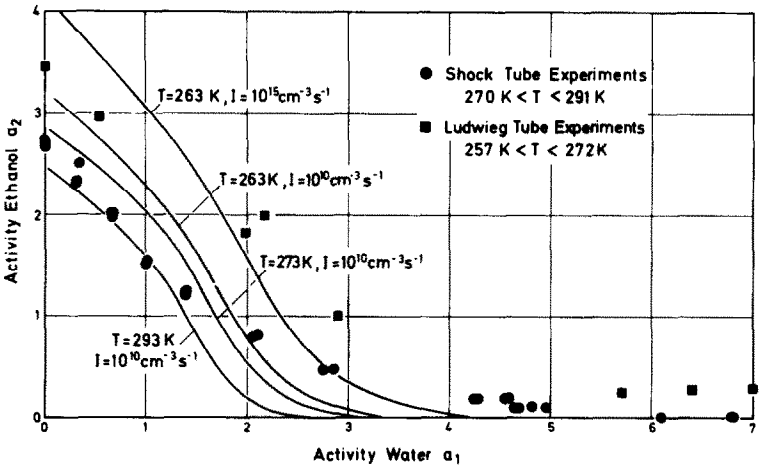

FIG. 7. Onset of nucleation for water–ethanol mixture—comparison of theory and experiments [8].

In extrapolating the nucleation path direction for the first step, the droplet growth is forced to have an increasing tendency.

Total liquid phase concentration is obtained by summing the individual masses over all drop classes. The two-phase mixture density therefore is equal to

$$\rho = \frac{\rho_0'' + \rho_1'' + \rho_2''}{1 - \sum_j [(N_j/\rho)_j \frac{4}{3}\pi r_j^3 \rho_j']}, \tag{73}$$

where the values $(N_j/\rho)_j$ are constant along the pathline and $N_j = J\Delta t_j$.

The drop mean radius is defined as

$$\bar{r} = \left\{ \sum_j [(N_j/\rho)_j \tfrac{4}{3}\pi r_j^3] \Big/ \sum_j (N_j/\rho)_j \right\}^{1/3}. \tag{74}$$

The change of the radius for small mass fractions $c_1' + c_2' < 10^{-3}$ is influenced by the droplet growth in the respective classes and the increase of the drop concentration by newly formed classes. The latent heat release causes a pressure increase for concentrations of approximately $c_1' + c_2' > 10^{-3}$ and a rapid quenching of the nucleation process. The increase of the mean radius under these conditions is accelerated as it depends only on the growth of the drops. The number of the drops remains constant and the concentration decreases slightly with the mixture dilution.

In the critical evaluation of the experimental and theoretical results it has to be taken into account, that application of the light extinction technique under our experimental conditions—i.e. tube diameter, wavelength, expansion rate, etc.—requires a particle concentration in excess of $10^{13}\,\mathrm{m}^{-3}$ which corresponds to a nucleation rate of approximately $10^{16}\,\mathrm{m}^{-3}\,\mathrm{s}^{-1}$. It is obvious that the drastic change in the concentration leads to deviations between the calculated and experimentally determined data. Considering this, the agreement in Fig. 8 is quite acceptable.

Despite the extremely fast change of concentration within the particulate drop from the critical value to the equilibrium composition within the time span of approximately 10^{-5} s, this demonstrates the capabilities of the model. With respect to the droplet growth

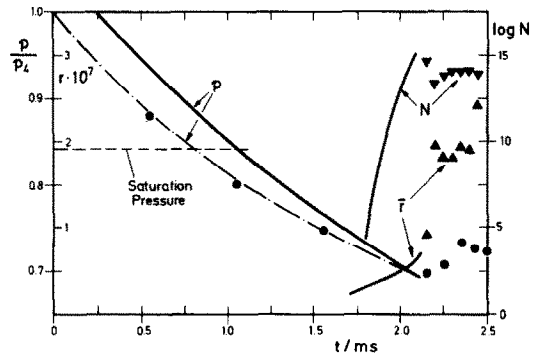

FIG. 8. Pressure trace, evolution of droplet mean radius and droplet concentration—comparison of theory and experiment for ethanol rich mixture. Initial conditions: $X_2'' = 0.70$, $p_4 = 1.98$ bar, $T_4 = 313.2$ K, $p_{12} = 0.09$ bar. Measurement points: ●, pressure; ▲, droplet radius; ▼, droplet concentration. Calculated parameters: —·—·—, at observation station; ———, along particle path.

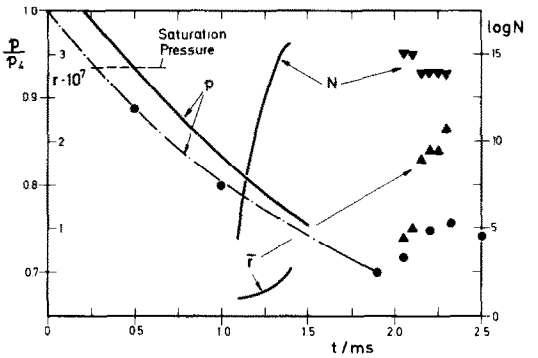

FIG. 9. Pressure trace, evolution of droplet mean radius and droplet concentration—comparison of theory and experiment for water rich mixture. Initial conditions: $X_2'' = 0.30$, $p_4 = 1.975$ bar, $T_4 = 314.1$ K, $p_{12} = 0.085$ bar. Measurement points: ●, pressure; ▲, droplet radius; ▼, droplet concentration. Calculated parameters: —·—·—, at observation station; ———, along particle path.

it should be emphasized that accurate measurements can only be expected down to 0.1 μm. This range on the other hand appears to be the upper limit of the validity of the calculations as the assumptions such as the thermal decoupling between gas phase and droplet will not hold. Still the agreement between the calculated and measured droplet size in this range is surprisingly good (Fig. 8) and is also dependent on the nucleation theory, not only on the droplet growth model.

Acknowledgements—Thanks are due to the Alexander von Humboldt Foundation for financial support, to Dr W. Studziński from the Institute of Fluid Flow Machinery, Polish Academy of Sciences, Gdańsk, and to the Deutsche Forschungsgemeinschaft (DFG).

REFERENCES

1. M. Bodmer, Korrosion durch Säuren in Dampfturbinen, *Brown Boveri Mitt.* **6,** 343–351 (1977).
2. G. Bohnsack, Spezielle Korrosivität aufgrund der Verteilungsverhältnisse im Zweiphasengebiet bei der Kondensation, *VGB Kraftwerkstechnik* **58,** 373–378 (1978).
3. G. J. Doyle, Self-nucleation in the sulfuric acid–water system, *J. Chem. Phys.* **35,** 795–799 (1961).
4. P. Mirabel and J. L. Katz, Binary homogeneous nucleation as a mechanism for the formation of aerosols, *J. Chem. Phys.* **60,** 1138–1144 (1973).
5. H. Flood, Tröpfchenbildung in übersättigten Äthylalkohol-Wasserdampfgemischen, *Z. Phys. Chem.* **A170,** 286–294 (1934).
6. H. Reiss, The kinetics of phase transitions in binary systems, *J. Chem. Phys.* **18,** 840–848 (1950).
7. D. Stauffer, Kinetic theory of two-component ("heteromolecular") nucleation and condensation, *J. Aerosol Sci.* **7,** 319–333 (1976).
8. R. A. Zahoransky and S. L. K. Wittig, Study of binary nucleation in a Ludwieg tube, *Proc. 13th Int. Symp. on Shock Tubes and Waves*, Niagara Falls, pp. 682–690 (1981).
9. C. Flageollet, M. Dinh Cao and P. Mirabel, Experimental study of nucleation in binary mixtures: the methanol–water and n-propanol–water systems, *J. Chem. Phys.* **72,** 544–549 (1980).
10. A. Kaser, Verhalten von Dämpfen löslicher Zweistoffgemische bei Expansion in Überschalldüsen-Tropfenkoaleszenz in einer Potential-Wirbelströmung, *Z. Angew. Math. Mech.* **53,** 39–56 (1973).
11. N. Fukuta and L. A. Walter, Kinetics of hydrometeorological growth from a vapor-spherical model, *J. Atmos. Sci.* **27,** 1160–1172 (1970).
12. N. A. Dingle, Rain scavenging of solid rocket exhaust clouds, NASA Report 2928, Grant NSG 1243, January (1978).
13. J. W. Meyer, Kinetic model for aerosol formation in rocket contrails, *AIAA J.* **17,** 135–144 (1979).
14. R. Zahoransky, Experimentelle Untersuchungen zur homogenen Kondensation löslicher Binärgemische, Ph.D. thesis, Lehrstuhl und Institut für Thermische Strömungsmaschinen, Universität Karlsruhe, Karlsruhe, Federal Republic of Germany (1982).
15. K. Neumann and W. Döring, Tröpfchenbildung in übersättigten Dampfgemischen zweier vollständig mischbarer Flüssigkeiten, *Z. Phys. Chem.* **A186,** 203–226 (1940).
16. G. Gyarmathy, The spherical droplet in gaseous carrier streams: review and synthesis, in *Multiphase Science and Technology* (edited by G. F. Hewitt, J. M. Delhaye and N. Zuber), Vol. 1, p. 99. Hemisphere, Washington, DC (1982).
17. G. Gyarmathy, Zur Wachstumsgeschwindigkeit kleiner Flüssigkeitstropfen in einer übersättigten Atmosphäre, *Z. Angew. Math. Phys.* **14,** 280–293 (1963).
18. K. Bro, S. L. K. Wittig and D. W. Sweeny, In situ optical measurements of particulate growth in sooting acetylene combustion, *Proc. 12th Int. Symp. on Shock Tubes and Waves*, pp. 429–436 (1979).
19. T. Teorell, Photometrische Messung der Konzentration und Dispersität in kolloidalen Lösungen II, *Kolloid. Z.* **54,** 58–66 (1931).
20. T. W. Lester and S. L. K. Wittig, Particle growth and concentration measurements in sooting homogeneous hydrocarbon combustion systems, *Proc. 10th Int. Shock Tube Symp.*, pp. 632–639 (1975).
21. D. Barschdorff, M. Neumann and S. Wiogo, Auswertung von Infrarotabsorptionsmessungen bei Blowdown-versuchen am Druckabbausystem des Reaktors Marviken, Report of Kernforschungszentrum Karlsruhe KFK 2534, Karlsruhe, Federal Republic of Germany (1977).
22. S. Wittig, R. Zahoransky and Kh. Sakbani, Die Dispersionsquotienten-Methode zur Bestimmung von Teilchengrößen im Sub-Micronbereich, *Proc. 8th Fachtagung der Gesellschaft für Aerosolforschung*, Schmallenberg, pp. 145–150 (1980).
23. J. P. Sislian and I. I. Glass, Condensation of water vapor in rarefaction waves: I. Homogeneous nucleation, *AIAA J.* **14,** 1731–1737 (1976).
24. I. I. Glass, S. P. Kalra and J. P. Sislian, Condensation of water vapor in rarefaction waves. III. Experimental results, *AIAA J.* **15,** 686–693 (1977).
25. D. Barschdorff, Carrier gas effects on homogeneous nucleation of water vapor in a shock tube, *Physics Fluids* **18,** 529–535 (1975).
26. P. Mirabel and J. L. Katz, Condensation of a supersaturated vapor IV. The homogeneous nucleation of binary mixtures, *J. Chem. Phys.* **67,** 1697–1704 (1977).

FORMATION ET CROISSANCE DE GOUTTELETTES DANS DES VAPEURS BINAIRES

Résumé—Un modèle antérieur de croissance de gouttelettes en condensation de corps pur est étendu à des mélanges binaires. Les résultats théoriques sont comparés avec des mesures dans la section d'un tube à choc utilisant des systèmes éthanol/eau. Les rayons de gouttelettes et la concentration sont déterminés au moyen de la technique du quotient de dispersion. On détermine des tailles de particules entre 0,1–1 μm et les densités entre 10^{11} et 10^{14} m^{-3}. Les résultats théoriques et expérimentaux sont en bon accord dans les conditions choisies.

TROPFENBILDUNG UND -WACHSTUM IN KONDENSIERENDEN BINÄREN DÄMPFEN

Zusammenfassung—Ein Tropfenwachstumsmodell für unäre Kondensation wurde auf binäre Gemische erweitert und mit experimentell ermittelten Werten verglichen. Die Expansion von Äthanol/Wasser-Lösungen im Hochdruckteil eines Stoßrohres führte zur Kondensation. Tropfenradius und -Konzentration wurden mit der Dispersions-Quotienten-Methode bestimmt. Die gemessene Partikelgröße liegt im Bereich 0,1–1 μm, die Partikeldichte zwischen 10^{11} und 10^{14} m^{-3}. Die theoretischen und experimentellen Ergebnisse stimmen gut überein. Auf Probleme wasserreicher Gemische wird eingegangen.

ОБРАЗОВАНИЕ И РОСТ КАПЕЛЬ ПРИ КОНДЕНСАЦИИ ПАРА БИНАРНЫХ ЖИДКОСТЕЙ

Аннотация—Предложенная ранее модель роста капель при конденсации однокомпонентной жидкости обобщена на случай бинарных смесей. Проведено сравнение результатов теоретического исследования с данными измерений, полученных на участке высокого давления ударной трубы со смесью этанол — вода. Радиусы и концентрация капель определялись методом дисперсии показателя преломления. Определены размеры капель в диапазоне от 0,1 мкм до 1 мкм и плотности концентрации от 10^{11} до 10^{14} $м^{-3}$. В рассматриваемых условиях теоретические результаты хорошо согласуются с экспериментальными данными.